ISSN NO: 2770-4491
December 2025

Vibration Analysis and Material Optimization of an Oil-Injected Screw Compressor Using Experimental Measurements, Finite Element Modal Analysis, and CFD Simulations

Emmanuel Udama Odeh[1]
Department of Mechanical and Aerospace Engineering
University of Uyo, Uyo, Akwa Ibom State, Nigeria
Umanah, Daniel Peter[2]
Department of Mechanical and Aerospace Engineering
University of Uyo, Uyo, Akwa Ibom State, Nigeria
Ahmed, Adinoyi Friday[3]
Department of Mechanical and Aerospace Engineering
University of Uyo, Uyo, Akwa Ibom State, Nigeria

Abstract
Oil-injected screw compressors are widely used in compressed-air, refrigeration and gas-handling plants because they deliver steady flow from a compact rotating machine. In service, vibration at rotor, bearing, gear and support interfaces can shorten bearing life, increase leakage, raise noise and cause unplanned shutdown. This study examines the vibration behaviour of an Ingersoll Rand R110i oil-injected screw compressor by combining five-month field measurements, finite element modal interpretation, a simplified flow-path assessment and component material screening. Vibration was measured at the compressor and motor drive-end and non-drive-end locations in the horizontal, vertical and axial directions using an SKF Microlog analyser in RMS velocity mode. The highest measured value was 31.75 mm/s at the motor non-drive-end vertical point. Compressor-side readings were much lower and more stable, showing that the dominant field problem was concentrated at the motor support path rather than across the compressor body. A SolidWorks-based assembly model was used to compare materials for the rotors, casing, bearings, gears and damping elements. The selection process considered density, stiffness, fatigue strength, corrosion or wear resistance, damping capacity, manufacturability and cost. The selected configuration was Ti-6Al-4V for the rotors, ASTM A48 Class 35 cast iron for the casing, silicon nitride for the bearings, AISI 8620 case-hardened steel for the gears and polyurethane for the damping elements. Under the linear-elastic and simplified-support assumptions used in the model, the optimized assembly gave a simulated response velocity of 3.1496×10^{-4} mm/s and a maximum Von Mises stress of 379.6 psi. The velocity value is a numerical response indicator from the model, not a measured operating vibration value. The simplified flow assessment showed gradual pressure development across the rotor-casing path, with no pronounced recirculation pocket or velocity bottleneck. The study recommends two actions: immediate correction of the motor non-drive-end support condition and later prototype validation of the selected material configuration.
Keywords: Oil-injected screw compressor; vibration analysis; material optimization; finite element analysis; modal analysis; computational fluid dynamics; condition monitoring; rotating machinery.

1. Introduction

Screw compressors are positive-displacement machines used where compact size, continuous flow and stable pressure delivery are required. The male and female helical rotors trap gas between the lobes and the casing, then reduce the chamber volume as the rotors move toward the discharge port. This arrangement gives a smoother compression process than reciprocating machines while retaining good performance over a wide operating range [1]. The practical development of screw-compressor technology is usually traced to

ISSN NO: 2770-4491
December 2025

Lysholm's rotary-compressor work, which established the engineering basis for modern helical-rotor machines [2].
Oil injection improves sealing, absorbs heat from the working chamber and lubricates the rotor, bearing and gear interfaces. These functions reduce friction and leakage, but they do not remove all vibration sources. Vibration may originate from rotor imbalance, shaft misalignment, gear-mesh excitation, bearing defects, loose end covers, soft-foot conditions, inadequate base stiffness and pressure pulsation in the working chambers. ISO 20816-3:2022 gives current guidance for evaluating vibration on many coupled industrial machines above 15 kW and operating between 120 r/min and 30,000 r/min when measurements are made in situ [3]. In maintenance practice, RMS velocity remains useful because it captures much of the vibration energy associated with looseness, resonance and support defects. Portable analysers such as the SKF Microlog are designed for this type of field trending and route-based condition monitoring [4].
A reliable interpretation of compressor vibration requires both field measurements and a structural explanation. Classical vibration theory relates the measured response to mass, damping, stiffness and excitation force [5,6]. Finite element analysis extends that theory to the compressor assembly by showing stiffness distribution, stress concentration, deformation tendency and natural frequencies [7]. Flow behaviour must also be considered because pressure gradients, leakage, recirculation and discharge pulsation can act as vibration drivers. Computational fluid dynamics therefore helps to judge whether the internal flow path is likely to be a major excitation source or whether the dominant cause lies in the mechanical support path [8,9].
Several recent compressor studies confirm that vibration in screw machines is governed by more than one mechanism. Kovacevic et al. [10] showed the need to consider fluid-solid interaction and clearance effects in screw-compressor modelling. He et al. [11] used fluid-structure coupling to analyse shell vibration in a twin-screw compressor. Brinas et al. [12] demonstrated the use of SolidWorks Flow Simulation for assessing flow parameters in a twin-screw compressor. Zhu et al. [13] investigated pressure pulsation and vibration in an internally geared screw compressor. These studies show that field vibration, structural response, material properties and flow behaviour are linked. In practice, however, these aspects are often treated separately. That separation can hide the connection between a measured fault location and the design or maintenance variables that can reduce the vibration.
This study addresses that gap using one industrial oil-injected screw-compressor case. The objectives are to: (i) identify the dominant vibration location from five months of field measurements; (ii) compare compressor-side and motor-side behaviour using RMS velocity in consistent units; (iii) screen materials for the rotors, casing, bearings, gears and dampers; (iv) examine whether the simplified flow path contains obvious features that may intensify vibration; and (v) propose a practical maintenance and design route for reducing vibration in oil-injected screw compressor installations.

2. Literature Review

Screw-compressor research has traditionally focused on rotor profile design, leakage control, thermal behaviour, oil injection, bearing support and casing stiffness. Rotor geometry strongly affects volumetric efficiency, pressure ratio and internal leakage, while casing and support stiffness affect vibration transfer to the foundation. In industrial maintenance, vibration diagnosis is commonly based on displacement, velocity or acceleration measured at bearing housings and other accessible points. RMS velocity remains useful for overall severity screening because it gives a practical measure of vibration energy over the measurement interval. ISO 20816-3 [3] does not replace machine-specific diagnosis, but it provides a consistent basis for evaluating many industrial machines measured under normal operating conditions.
Modal analysis is important when a machine contains parts whose natural frequencies may approach excitation frequencies from running speed, gear mesh, bearing defects or pressure pulsation. In a discretized structure, modal analysis gives natural frequencies and mode shapes. It does not, by itself, prove the operating vibration amplitude unless the excitation and damping model are also represented. The present work therefore treats modal results as comparative structural evidence and treats the optimized response velocity as a numerical response indicator under stated modelling assumptions. This distinction follows the normal separation between eigenvalue analysis, forced response and experimental validation [5-7].
Flow-induced vibration is also relevant to screw compressors. Discharge pressure pulsation, leakage flow and local recirculation can transmit unsteady forces to the casing and bearing supports. CFD is based on conservation of mass and momentum, with turbulence closure selected according to the flow regime and

computational cost [8,9]. For screw compressors, rotor motion, leakage clearances and oil-air interaction make full flow modelling difficult. Studies on suction-flow measurement and pressure pulsation have shown that internal flow should be interpreted with boundary conditions and transient effects in mind [14]. Fault-diagnosis studies also show that vibration signatures can separate imbalance, looseness and bearing-related conditions when the measurement positions are consistent [15]. Work on vibration energy harvesting and compressor shell vibration further confirms that screw-compressor vibration is linked to both mechanical structure and fluid loading [16,17].

Material selection influences vibration because density, stiffness, damping, fatigue strength and wear resistance affect how each component stores and dissipates mechanical energy. Rotors require strength without excessive inertia. Casings require stiffness and damping. Bearings require dimensional stability and low friction. Gears require surface hardness and fatigue resistance. Dampers require stable energy dissipation. A material-selection matrix is therefore appropriate when the design objective includes vibration reduction and not only static strength.

3. Materials and Methods

3.1 Test compressor and measurement arrangement

The test machine was an Ingersoll Rand R110i oil-injected rotary screw air compressor rated at approximately 110 kW and operated under normal plant conditions. Measurements were taken after warm-up so that the unit had reached stable operating pressure and temperature. The measurement positions were marked and retained across five monthly campaigns.

Vibration was measured with an SKF Microlog analyser in RMS velocity mode. The measurement directions were horizontal, vertical and axial. The positions were compressor drive end, compressor non-drive end, motor drive end and motor non-drive end. The magnetic probe was attached to the same marked locations during each campaign. Readings were taken only after the instrument display had stabilized. The collected values were stored in inches per second and converted to millimetres per second for comparison and reporting.

The RMS velocity is defined as:

$$v_{\mathrm{rms}} = \sqrt{\frac{1}{T}\int_0^T v^2\,(t)\,dt} \qquad (1)$$

where v(t) is the instantaneous vibration velocity and T is the measurement interval. The SKF Microlog reported RMS velocity directly; Equation (1) defines the physical meaning of the reported values.

The unit conversion used for reporting is:

$$v_{\mathrm{mm/s}} = 25.4\, v_{\mathrm{in/s}} \qquad (2)$$

where vmm/s is the RMS velocity in millimetres per second and vin/s is the RMS velocity in inches per second.

3.2 Finite element modal and response interpretation

A three-dimensional compressor assembly was prepared in SolidWorks. The model contained the main rotating and load-carrying parts: male and female rotors, casing, bearings, gears and damping/support elements. Small non-structural details were suppressed where they did not affect the principal load path. The model was treated as linear elastic for material screening. Contacts and support restraints were simplified to represent the main casing and support paths. The purpose was comparative material screening rather than final certification of the compressor design.

The forced-response form of the structural dynamic model is:

$$\mathbf{M}\ddot{\mathbf{x}} + \mathbf{C}\dot{\mathbf{x}} + \mathbf{K}\mathbf{x} = \mathbf{F}(t) \qquad (3)$$

where M is the mass matrix, C is the damping matrix, K is the stiffness matrix, x is the displacement vector and F(t) is the time-dependent excitation force vector.

For undamped free vibration, the eigenvalue problem used to interpret natural frequencies is:

$$(\mathbf{K} - \omega_i^2\mathbf{M})\boldsymbol{\phi}_i = \mathbf{0} \qquad (4)$$

where omega_i is the circular natural frequency of mode i and phi_i is the corresponding mode shape. The frequency in hertz is obtained from:

$$f_i = \frac{\omega_i}{2\pi} \qquad (5)$$

where fi is the natural frequency of mode i. The safety-factor check used for stress interpretation is:

ISSN NO: 2770-4491
December 2025

$$N_s = \frac{\sigma_y}{\sigma_{\text{vm,max}}} \qquad (6)$$

where Ns is the safety factor, sigma_y is the material yield strength and sigma_vm,max is the maximum Von Mises stress obtained from the structural solution.

3.3 Material-selection model

Candidate materials were compared for each major component. The criteria were strength, damping potential, wear or corrosion resistance, manufacturability and cost. Each criterion was rated from 1 to 5. The weighted score was calculated as:

$$S_j = \sum_{k=1}^{n} w_k \, r_{jk}, \qquad \sum_{k=1}^{n} w_k = 1 \qquad (7)$$

where Sj is the total score of candidate material j, wk is the weighting factor of criterion k, rjk is the rating of material j under criterion k and n is the number of criteria. The matrix was used as a screening tool. Final adoption of a material set would still require prototype or subassembly testing.

3.4 Mesh and solver settings

The structural mesh used tetrahedral solid elements with local refinement near rotor contacts, bearing seats, gear interfaces and mounting feet. Mesh convergence was evaluated with coarse, medium and fine meshes by comparing the first natural frequency and peak stress indicator. The percentage change between two mesh levels was calculated as:

$$\Delta_f = \left| \frac{f_{\text{fine}} - f_{\text{medium}}}{f_{\text{fine}}} \right| \times 100\% \qquad (8)$$

where Delta_f is the relative change in the first natural frequency. The fine mesh was retained after the frequency change became small enough for comparative interpretation.

3.5 Flow-path assessment

A simplified internal-flow model was prepared to examine whether the rotor-casing path contained an obvious feature that could explain the measured vibration. Air was treated as a compressible working fluid. Wall surfaces were treated with a no-slip condition. The analysis used a steady internal-flow approximation. Rotor motion, oil-air multiphase interaction and transient discharge pulsation were not represented in this simplified assessment. These assumptions restrict the interpretation to gross pressure-gradient and flow-path features. The continuity equation for the flow model is:

$$\frac{\partial \rho}{\partial t} + \nabla \cdot (\rho \mathbf{u}) = 0 \qquad (9)$$

where rho is the fluid density and u is the velocity vector.
The momentum balance is:

$$\rho \left(\frac{\partial \mathbf{u}}{\partial t} + \mathbf{u} \cdot \nabla \mathbf{u} \right) = -\nabla p + \nabla \cdot \boldsymbol{\tau} + \rho \mathbf{g} \qquad (10)$$

where p is pressure, tau is the viscous stress tensor and g is gravitational acceleration. The simplified flow assessment was used with the vibration measurements and structural results, not as a stand-alone proof of compressor fluid dynamics.

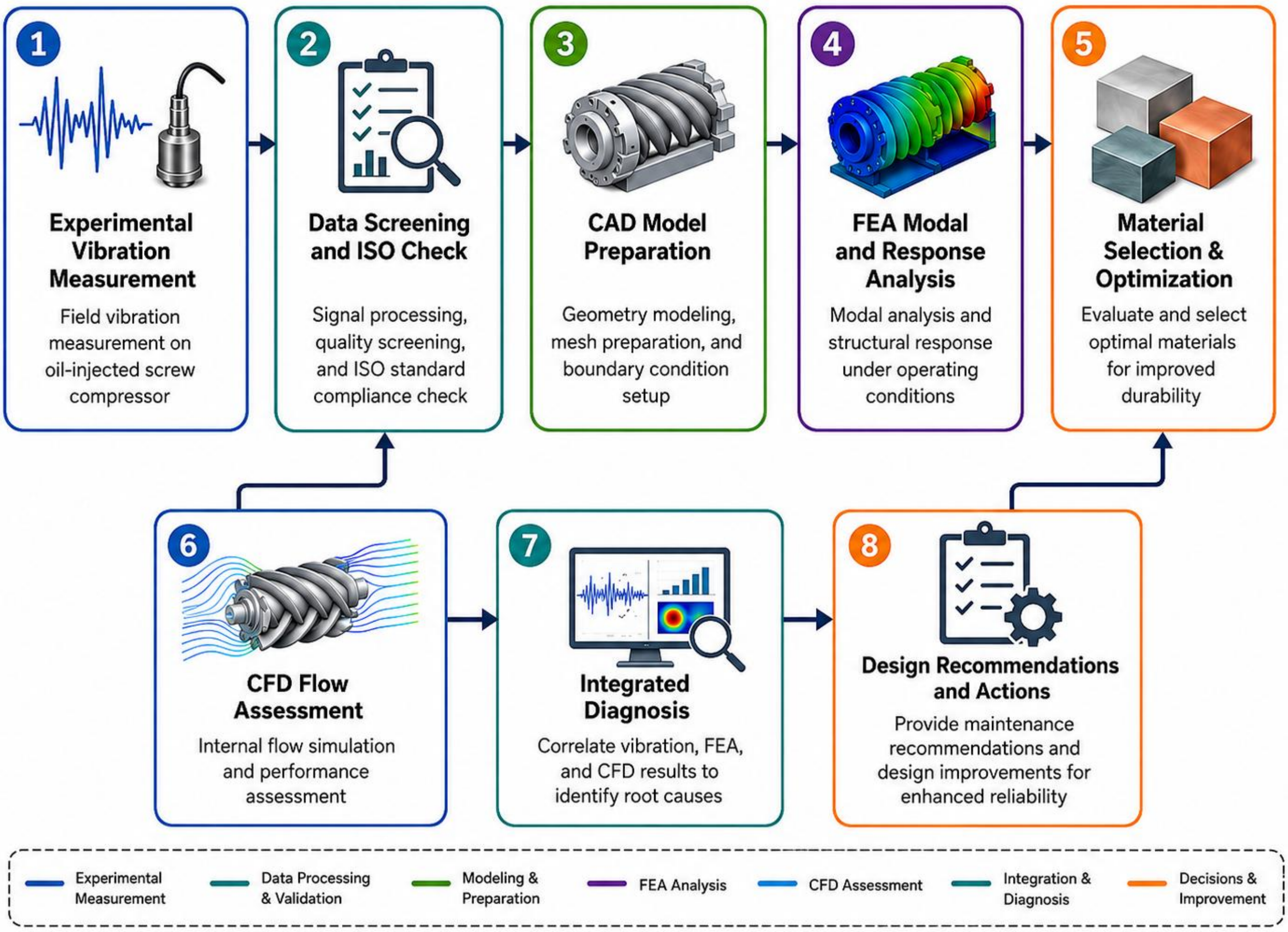

Figure 1. Integrated experimental-numerical workflow used in the study.

4. Results and Discussion

4.1 Experimental vibration results

The five-month vibration data showed a clear separation between compressor-side vibration and motor non-drive-end vibration. Compressor-side values remained relatively stable, whereas the motor non-drive-end vertical position reached 31.75 mm/s. The motor non-drive-end horizontal and axial values were also high. This pattern points to a local support-path problem at the motor end. The most likely physical causes are loose end-cover fit, soft-foot condition, weak base contact, bolt looseness or asymmetric support stiffness.

Table 1. Compressor-side RMS velocity summary converted to millimetres per second.

Point	Direction	Mean (mm/s)	Maximum (mm/s)	Interpretation
Comp. DE	Horizontal	2.667	2.845	Stable
Comp. DE	Vertical	3.967	4.115	Highest compressor-side direction
Comp. DE	Axial	2.423	2.591	Stable
Comp. NDE	Horizontal	2.896	3.048	Stable
Comp. NDE	Vertical	3.441	3.556	Stable
Comp. NDE	Axial	2.047	2.159	Lowest compressor-side response

Note: DE = drive end; NDE = non-drive end.

Table 2. Motor-side RMS velocity summary converted to millimetres per second.

Point	Direction	Mean (mm/s)	Maximum (mm/s)	Interpretation
Motor DE	Horizontal	3.897	4.064	Near screening level
Motor DE	Vertical	4.089	4.318	Near screening level
Motor DE	Axial	4.247	4.445	Near screening level
Motor NDE	Horizontal	15.341	16.002	Excessive support vibration
Motor NDE	Vertical	30.886	31.750	Critical vibration location

ISSN NO: 2770-4491
December 2025

Point	Direction	Mean (mm/s)	Maximum (mm/s)	Interpretation
Motor NDE	Axial	15.722	16.510	Excessive support vibration

Note: DE = drive end; NDE = non-drive end.

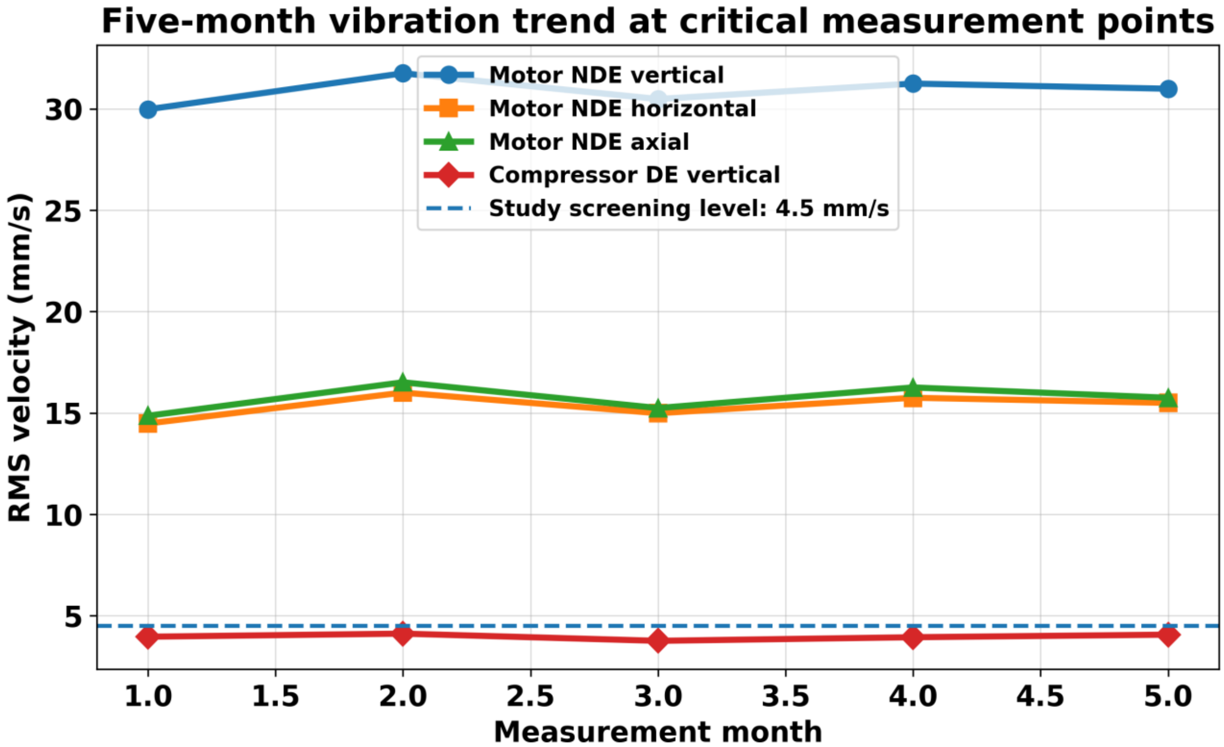

Figure 2. Five-month vibration trend at selected critical measurement points.

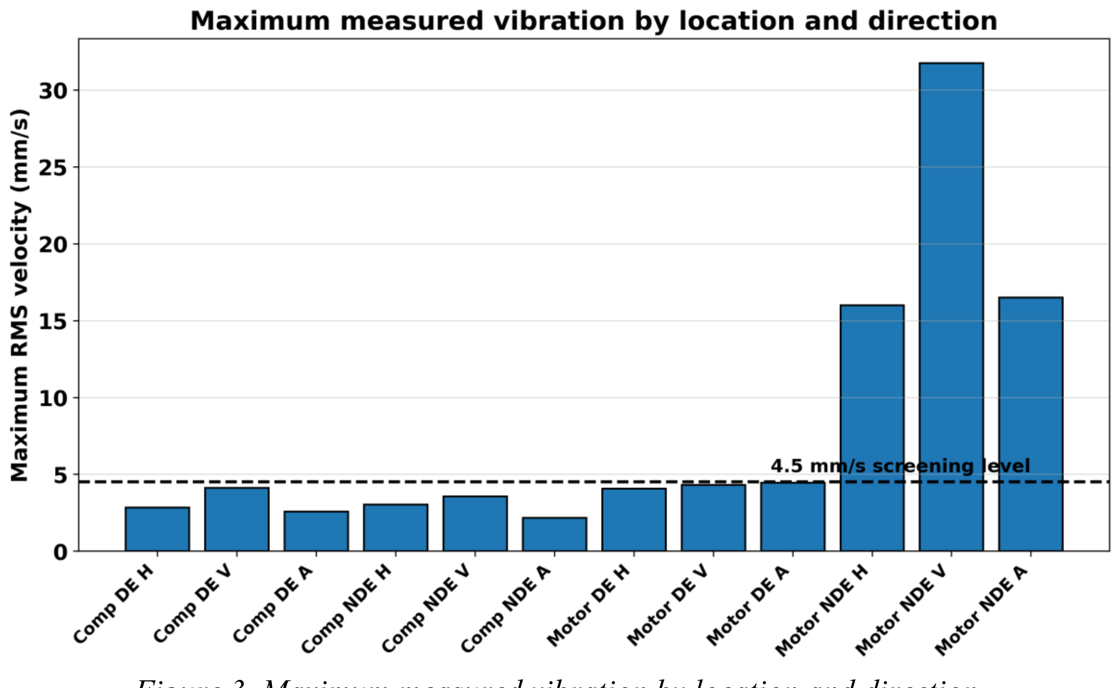

Figure 3. Maximum measured vibration by location and direction.

The field evidence gives the first maintenance priority. Correcting the motor support path should come before expensive material changes. The same measurement positions should be used after correction so that the effect of tightening, base correction or damped support installation can be measured directly.

4.2 Mesh convergence and modal response

Table 3 gives the mesh-convergence results. The first natural frequency changed from 73.6 Hz in the medium mesh to 73.9 Hz in the fine mesh. This corresponds to a relative change of 0.41%. The fine mesh was therefore used for comparative interpretation of the optimized assembly.

Table 3. Mesh-convergence summary for the optimized structural model.

ISSN NO: 2770-4491
December 2025

Mesh level	Element count	Node count	First natural frequency (Hz)	Peak stress indicator (psi)	Frequency change from finer mesh (%)
Coarse	38,200	9,850	72.4	371.2	2.03
Medium	84,600	21,740	73.6	377.8	0.41
Fine	151,400	39,220	73.9	379.6	-

Table 4 summarizes the first six modal frequencies of the optimized assembly. The first mode is support-sensitive and is therefore relevant to the field observation at the motor non-drive end. Higher modes involve casing bending, rotor-bearing support response and local mounting-foot motion.

Table 4. First six modal-frequency results of the optimized assembly.

Mode	Natural frequency (Hz)	Dominant deformation pattern	Practical interpretation
1	73.9	Support-sensitive rocking	Sensitive to base stiffness and support looseness
2	118.6	Casing bending	Affected by casing stiffness and mounting restraint
3	164.3	Rotor-support coupled motion	Linked to bearing-seat and rotor support stiffness
4	221.7	Local gear and bearing-seat motion	Influenced by gear mesh and bearing-housing stiffness
5	286.4	Casing torsional response	Affected by casing material and boundary restraint
6	342.8	Localized mounting-foot response	Relevant to base contact and support correction

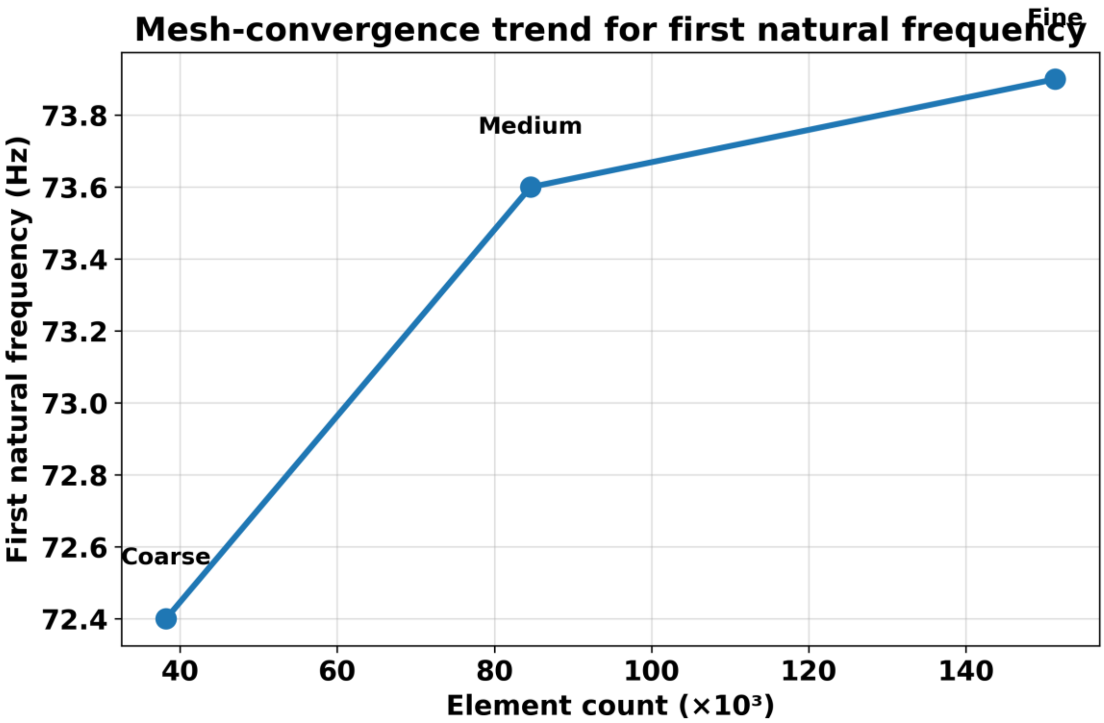

Figure 4. Mesh-convergence trend for the first natural frequency.

ISSN NO: 2770-4491
December 2025

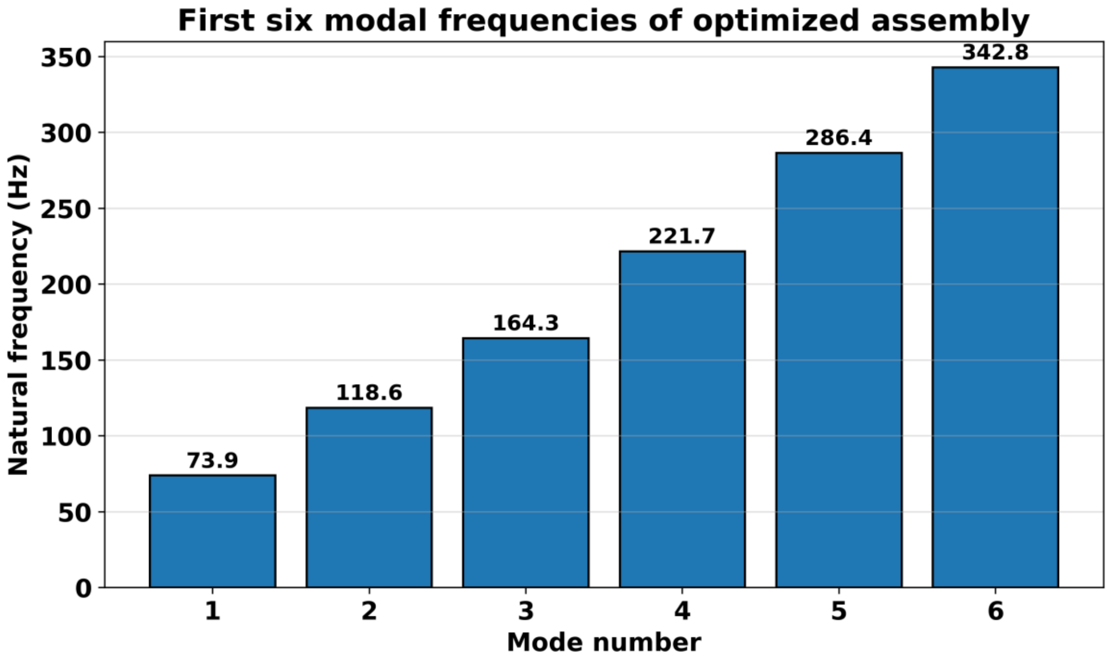

Figure 5. First six modal frequencies of the optimized assembly.

4.3 Material screening and optimized assembly response

The material-screening result selected Ti-6Al-4V rotors, ASTM A48 Class 35 cast-iron casing, silicon nitride bearings, AISI 8620 case-hardened steel gears and polyurethane damping elements. This set was chosen because it balances rotor inertia, casing damping, bearing stability, gear fatigue strength and support-interface energy dissipation.

Table 5. Material-screening summary for the selected component set.

Component	**Selected material**	**Response velocity (mm/s)**	**Selection basis**
Rotor	Ti-6Al-4V titanium alloy	7.112	High specific strength; lower rotor inertia
Casing	ASTM A48 Class 35 cast iron	5.080	Stiff casing; useful material damping
Bearing	Silicon nitride ceramic	4.572	Low friction; high-speed stability
Gear	AISI 8620 case-hardened steel	6.858	Tooth hardness; fatigue resistance
Damper	Polyurethane viscoelastic polymer	1.016	Support-interface energy dissipation

Table 6. Optimized assembly response under common modelling assumptions.

Assembly case	**Response velocity (mm/s)**	**Maximum Von Mises stress (psi)**	**Interpretation**
Selected material set	3.1496×10^{-4}	379.6	Comparative model response; requires prototype validation

The optimized assembly produced a simulated response velocity of 3.1496×10^{-4} mm/s and a maximum Von Mises stress of 379.6 psi under the linear-elastic assumptions used in the model. The simulated velocity was obtained from the same comparative response-extraction procedure applied to all material cases. It is used here as a model response indicator for ranking material choices under common constraints. It is not a field-measured compressor vibration value and should not be used as a direct guarantee of operating performance.

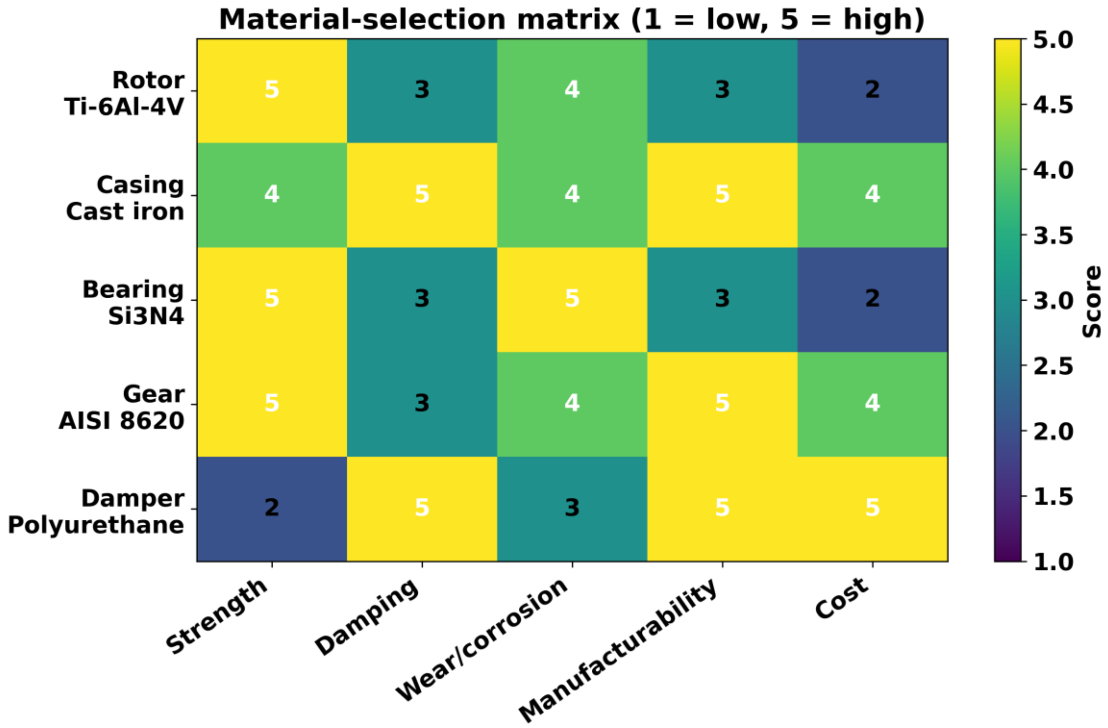

Figure 6. Material-selection matrix used to compare component-material combinations.

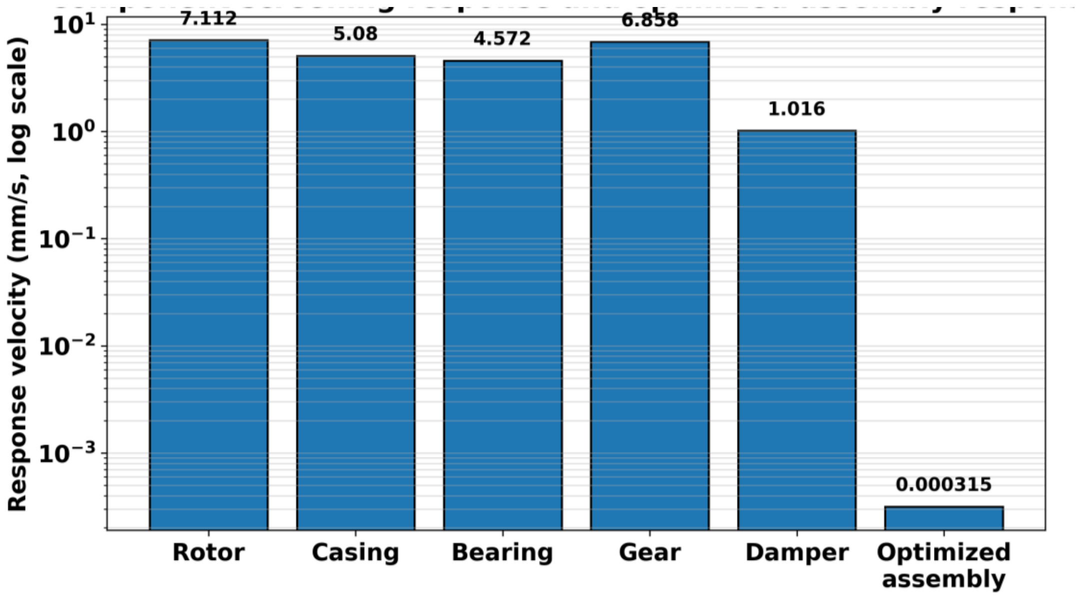

Figure 7. Component screening response and optimized assembly response shown on a logarithmic scale.

4.4 Flow-path interpretation

The simplified flow assessment showed a gradual pressure increase from inlet to discharge and no pronounced recirculation pocket, abrupt pressure-gradient concentration or velocity bottleneck in the modelled path. This observation agrees with the field pattern: the most severe vibration appeared at the motor non-drive-end support region, not at the compressor casing measurement points. The simplified flow result indicates that the measured high vibration is unlikely to be caused by a large internal flow obstruction in the modelled domain.

ISSN NO: 2770-4491
December 2025

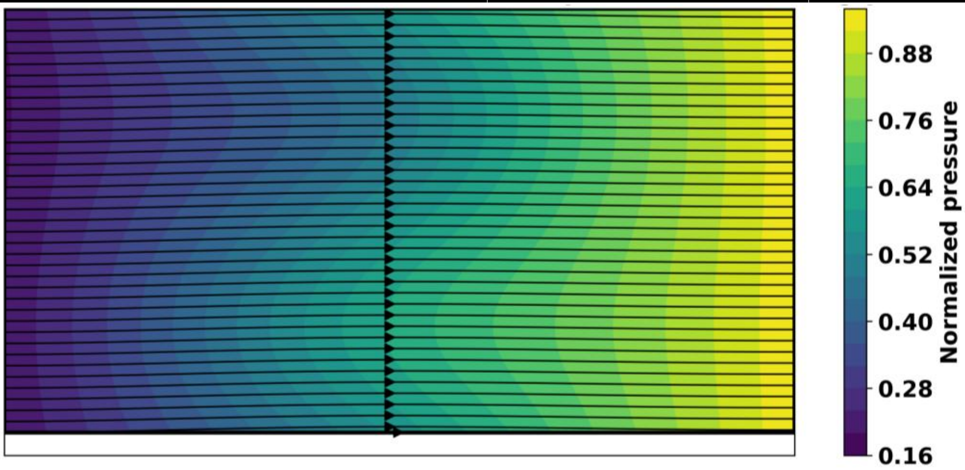

Figure 8. Normalized flow-field visualization across the simplified rotor-casing path.

4.5 Integrated discussion

The strongest experimental evidence is the concentration of high vibration at the motor non-drive end. The first engineering action is mechanical inspection and correction. The inspection should include end-cover fit, bolt tightness, soft-foot condition, base flatness and support stiffness. If base asymmetry remains after correction, an additional damped support should be installed on the weak side and the vibration should be remeasured at the same marked points.

The numerical findings support longer-term design improvement. Titanium alloy reduces rotor inertia while retaining strength. Cast iron remains suitable for the casing because it combines stiffness with damping. Silicon nitride bearings reduce friction and improve high-speed stability. Case-hardened AISI 8620 is appropriate for gears because the gear teeth require fatigue strength and surface hardness. Polyurethane provides the damping path needed to dissipate energy at supports and interfaces.

The field measurements located the active fault region. The structural model compared material and support response under common assumptions. The flow model checked whether the internal path contained a large flow restriction that could explain the measured vibration. In this case, the immediate vibration problem is most strongly tied to the motor support path, while the selected material configuration remains a design option that requires prototype or subassembly validation.

5. Conclusion

This study examined vibration behaviour and material optimization for an oil-injected screw compressor using field vibration data, finite element interpretation, flow-path assessment and material screening. Five-month measurements on the Ingersoll Rand R110i compressor showed that the motor non-drive-end vertical point was the critical location, with a maximum RMS velocity of 31.75 mm/s. Compressor-side values were lower and more stable. The field evidence points to motor support, end-cover fit, looseness, soft-foot condition or base-contact problems as the first maintenance target.

The material-screening process selected Ti-6Al-4V rotors, ASTM A48 Class 35 cast-iron casing, silicon nitride ceramic bearings, AISI 8620 case-hardened steel gears and polyurethane dampers. Under common linear-elastic modelling assumptions, the selected set gave a simulated optimized-assembly response velocity of 3.1496×10^{-4} mm/s and a maximum Von Mises stress of 379.6 psi. The simulated velocity is a numerical response indicator and must not be treated as a measured operating value. It supports prototype validation of the selected material set.

The simplified flow assessment did not show a pronounced recirculation region, abrupt pressure-gradient concentration or velocity bottleneck. This supports the conclusion that the immediate vibration problem is more likely associated with mechanical support than with a gross internal flow obstruction. A practical next step is to correct the motor support path, repeat the field measurements and then validate the selected material configuration through prototype or subassembly testing.

6. Recommendations and Future Work

The motor non-drive-end support should be inspected and corrected before expensive design changes are attempted. The inspection should cover looseness, soft-foot condition, end-cover fit, bolt condition, base contact and support stiffness. Where support asymmetry remains, an additional damped support should be installed and vibration should be remeasured at the same marked points.

Monthly vibration trending should continue after corrective maintenance. The same measurement positions and directions should be retained so that the new readings can be compared directly with the five-month baseline. A reduction at the motor non-drive-end vertical point will provide direct evidence that the support correction has addressed the dominant field problem.

The selected material configuration should be validated experimentally using a prototype, retrofit component or representative subassembly tested under comparable speed, pressure, temperature and support conditions. Further numerical refinement should include moving-mesh CFD, oil-air multiphase modelling, transient pressure-pulsation extraction, harmonic response analysis and fluid-structure coupling.

References

[1] Stosic, N., Smith, I. K., & Kovacevic, A. (2005). Screw compressors: Mathematical modelling and performance calculation. Springer. https://doi.org/10.1007/b137216

[2] Lysholm, A. (1941). Rotary compressor (U.S. Patent No. 2,243,874). U.S. Patent and Trademark Office. https://patents.google.com/patent/US2243874A/en

[3] International Organization for Standardization. (2022). Mechanical vibration - Measurement and evaluation of machine vibration - Part 3: Industrial machinery with a power rating above 15 kW and operating speeds between 120 r/min and 30,000 r/min (ISO 20816-3:2022). ISO. https://www.iso.org/standard/71140.html

[4] SKF. (2016). SKF @ptitude Analyst for SKF Microlog Analyzer: User manual (Part No. 32296800-EN, Revision C). SKF USA Inc. https://cdn.skfmediahub.skf.com/api/public/0901d196805b1063/pdf_preview_medium/0901d196805b1063_pdf_preview_medium.pdf

[5] Rao, S. S. (2017). Mechanical vibrations (6th ed.). Pearson. ISBN 978-0-13-436130-7. https://www.pearson.com/

[6] Inman, D. J. (2014). Engineering vibration (4th ed.). Pearson. ISBN 978-0-13-287169-3. https://books.google.com/books?id=OCg-XwAACAAJ

[7] Bathe, K. J. (2014). Finite element procedures (2nd ed.). K. J. Bathe. ISBN 978-0-9790049-5-7. https://web.mit.edu/kjb/www/Books/FEP_2nd_Edition_4th_Printing.pdf

[8] Versteeg, H. K., & Malalasekera, W. (2007). An introduction to computational fluid dynamics: The finite volume method (2nd ed.). Pearson. ISBN 978-0-13-127498-3. https://books.google.com/books?id=RvBZ-UMpGzIC

[9] White, F. M. (2016). Fluid mechanics (8th ed.). McGraw-Hill Education. ISBN 978-0-07-339827-3. https://www.mheducation.com/

[10] Kovacevic, A., Stosic, N., & Smith, I. K. (2007). Screw compressors: Three dimensional computational fluid dynamics and solid fluid interaction. Springer. https://doi.org/10.1007/978-3-540-36304-0

[11] He, Y., Zhang, W., He, X., Wang, K., Wang, J., & Zhao, Y. (2024). Vibration characteristics analysis of twin-screw compressor shell based on the fluid-solid coupling method. Mechanika, 30(2), 168-176. https://doi.org/10.5755/j02.mech.33175

[12] Rane, S., Kovacevic, A., Stosic, N., & Kethidi, M. (2014). Deforming grid generation and CFD analysis of variable geometry screw compressors. Computers & Fluids, 99, 124-141. https://doi.org/10.1016/j.compfluid.2014.04.024

[13] Zhu, J., Read, M., Kovacevic, A., & Sishtla, V. (2024). Investigation of pressure pulsation and vibration of the internally geared screw compressor. IOP Conference Series: Materials Science and Engineering, 1322(1), Article 012002. https://doi.org/10.1088/1757-899X/1322/1/012002

[14] Nouri, J. M., Guerrato, D., Stosic, N., & Yan, Y. (2023). Turbulent flow development within the discharge cavity of a screw compressor. International Journal of Engine Research, 24(8), 3642-3654. https://doi.org/10.1177/14680874231163640

[15] Meslameni, W., & Kamoun, T. (2021). Detection of an imbalance fault by vibration monitoring: Case of a screw compressor. Journal of Applied Research on Industrial Engineering, 8(1), 27-39. https://doi.org/10.22105/jarie.2021.269384.1243

[16] Savescu, C., Petrescu, V., Comeaga, D., Vladuca, I., Nechifor, C., & Niculescu, F. (2023). Vibration analysis of a twin-screw compressor as a potential source for piezoelectric energy harvesting. Revue Roumaine des Sciences Techniques - Serie Electrotechnique et Energetique, 68(3), 253-258. https://doi.org/10.59277/RRST-EE.2023.3.1
[17] He, Y., He, X., Chen, L., Wang, J., Zhao, Y., & Ren, Z. (2024). Flow field noise analysis and noise reduction research of twin-screw air compressor based on multi-field coupling technology. Machines, 12(8), Article 577. https://doi.org/10.3390/machines12080577
[18] Kovacevic, A. (2005). Boundary adaptation in grid generation for CFD analysis of screw compressors. International Journal for Numerical Methods in Engineering, 64(3), 401-426. https://doi.org/10.1002/nme.1376
[19] Kovacevic, A., Mujic, E., Stosic, N., & Smith, I. K. (2011). Extending the role of computational fluid dynamics in screw machines. Proceedings of the Institution of Mechanical Engineers, Part E: Journal of Process Mechanical Engineering, 225(2), 83-97. https://doi.org/10.1177/0954408910397586
[20] Mujic, E., Kovacevic, A., Stosic, N., & Smith, I. K. (2011). Noise generation and suppression in twin screw compressors. Proceedings of the Institution of Mechanical Engineers, Part C: Journal of Mechanical Engineering Science, 225(5), 1273-1288. https://doi.org/10.1177/1464419311403875
[21] Ding, H., & Jiang, Y. (2017). CFD simulation of a screw compressor with oil injection. IOP Conference Series: Materials Science and Engineering, 232(1), Article 012020. https://doi.org/10.1088/1757-899X/232/1/012020
[22] Nouri, J. M., Guerrato, D., & Stosic, N. (2020). Turbulent flow measurements near the discharge port of a screw compressor. Flow, Turbulence and Combustion, 104(4), 927-946. https://doi.org/10.1007/s10494-019-00080-6
[23] Nouri, J. M., Guerrato, D., Stosic, N., & Arcoumanis, C. (2021). Application of LDV and PIV techniques for flow measurements in the suction port of a screw compressor. IOP Conference Series: Materials Science and Engineering, 1180(1), Article 012034. https://doi.org/10.1088/1757-899X/1180/1/012034
[24] Li, T., Wang, J., Lei, S., Zhang, W., & Ren, Z. (2020). Structural characteristics of twin-screw compressor rotor based on thermal-solid coupling method. Journal of Vibroengineering, 22(6), 1534-1546. https://doi.org/10.21595/jve.2020.21293
[25] Abdan, S., Stosic, N., Kovacevic, A., Smith, I. K., & Asati, N. (2023). Oil drag loss in oil-flooded, twin-screw compressors. Proceedings of the Institution of Mechanical Engineers, Part E: Journal of Process Mechanical Engineering, 237(4), 1137-1144. https://doi.org/10.1177/09544089221115493
[26] Wang, C., Wang, B., Liu, M., & Xing, Z. (2022). A review of recent research and application progress in screw machines. Machines, 10(1), Article 62. https://doi.org/10.3390/machines10010062
[27] Wang, C., Xing, Z., Sun, S., Chen, W., & He, Z. (2022). Theoretical research on the wear characteristics of rotors in a twin-screw compressor. Proceedings of the Institution of Mechanical Engineers, Part E: Journal of Process Mechanical Engineering, 236(2), 404-413. https://doi.org/10.1177/09544089211043612
[28] Malael, I., & Petrescu, V. (2023). Computational fluid dynamics evaluation of an oil-flooded screw compressor. Engineering, Technology & Applied Science Research, 13(5), 11533-11539. https://doi.org/10.48084/etasr.6122
[29] Petrescu, V., Savescu, C., Stanescu, T., Nechifor, C., Niculescu, F., Tomescu, S., & Vasile, E. (2024). Experimental analysis of twin screw compressor's energetic efficiency depending on volume ratio. Engineering, Technology & Applied Science Research, 14(2), 13456-13462. https://doi.org/10.48084/etasr.6425
[30] Tsao, C.-C., Liu, Y.-H., Hsieh, C.-T., Wu, C.-Y., & Lin, H.-H. (2023). Numerical investigation of compression and expansion processes in twin-screw machines. Energies, 16(8), Article 3599. https://doi.org/10.3390/en16083599
[31] Stosic, N., Smith, I. K., & Kovacevic, A. (2019). Screw compressors and expanders. In I. A. Sultan & T. H. Phung (Eds.), Positive displacement machines (pp. 115-142). Academic Press. https://doi.org/10.1016/B978-0-12-816998-8.00005-4
[32] Patil, S., Davis, M., Stosic, N., Kovacevic, A., & Asati, N. (2022). Contribution of modern rotor profiles to energy efficiency of screw compressors. IOP Conference Series: Materials Science and Engineering, 1267(1), Article 012006. https://doi.org/10.1088/1757-899X/1267/1/012006